# Seismic evidence for uniform crustal accretion along slow-spreading ridges in the equatorial Atlantic Ocean

**Zhikai Wang* and Satish C. Singh**

Institut de Physique du Globe de Paris, 1 rue Jussieu, Paris 75238, France

*Corresponding author: zwang@ipgp.fr

# Supplementary Information

**This PDF file includes:**

Supplementary Figures 1 to 9;

Supplementary Tables 1 to 4;

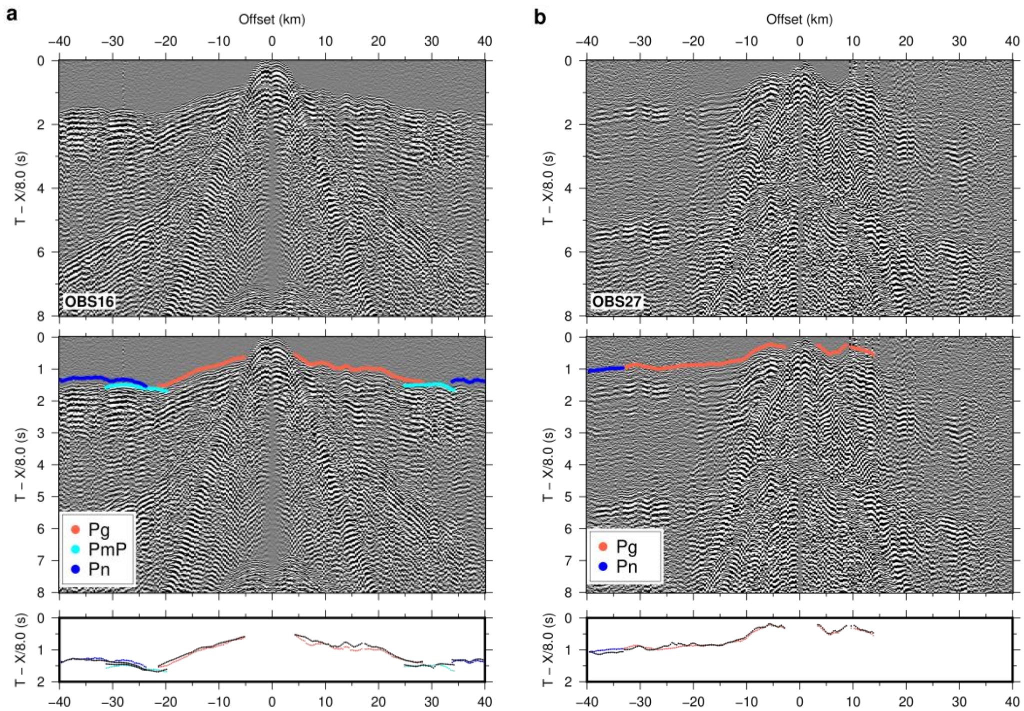


**Supplementary Fig. 1. OBS data and P-wave arrivals (Pg, PmP and Pn).** **a**, OBS16 and **b**, OBS27. Top: Receiver gathered seismic data after band-pass filtering plotted at reduced travel time using a reduction velocity of 8.0 km. Middle: Receiver gathered seismic data with the travel time picks. Bottom: Comparisons of the picked travel times and modelled travel times (black dots). The effects of bathymetry variation are removed in all plots by subtracting the vertical propagation time in water beneath each source, assuming a water velocity of 1.5 km/s.

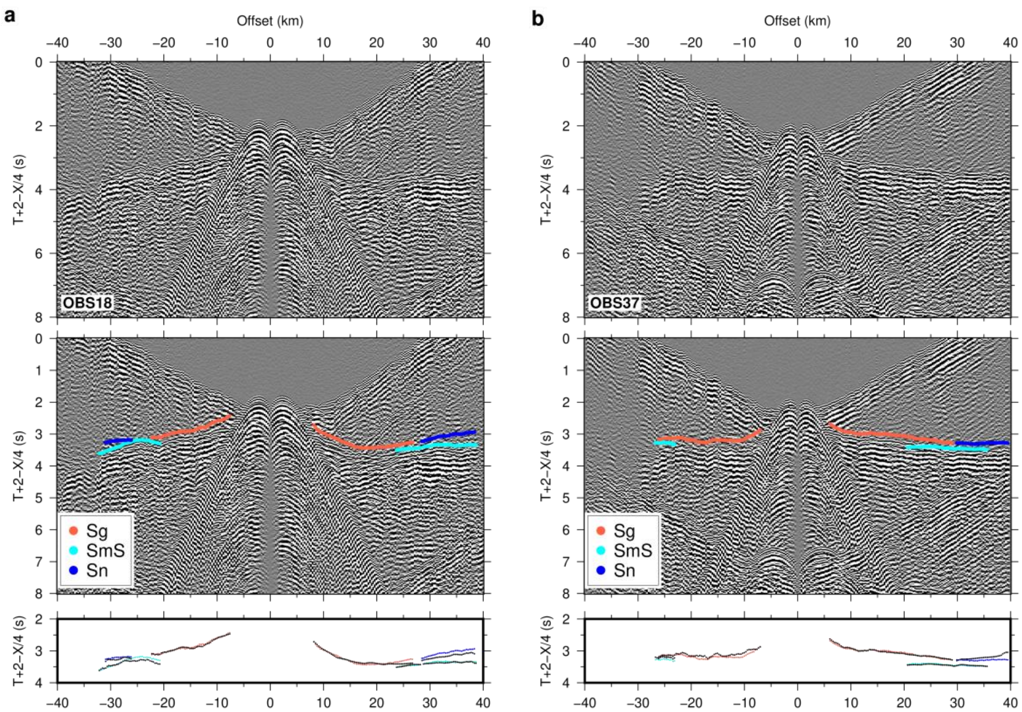


**Supplementary Fig. 2. OBS data and S-wave arrivals (Sg, SmS and Sn). a**, OBS18 and **b**, OBS37. Top: Receiver gathered seismic data after band-pass filtering plotted at reduced travel time using a reduction velocity of 4.0 km/s. To better show the seismic section, we shift the data by 2 s. Middle: Receiver gathered seismic data with the travel time picks. Bottom: Comparisons of the picked travel times and modelled travel times (black dots). The effects of bathymetry variation are removed in all plots by subtracting the vertical propagation time in water beneath each source, assuming a water velocity of 1.5 km/s.

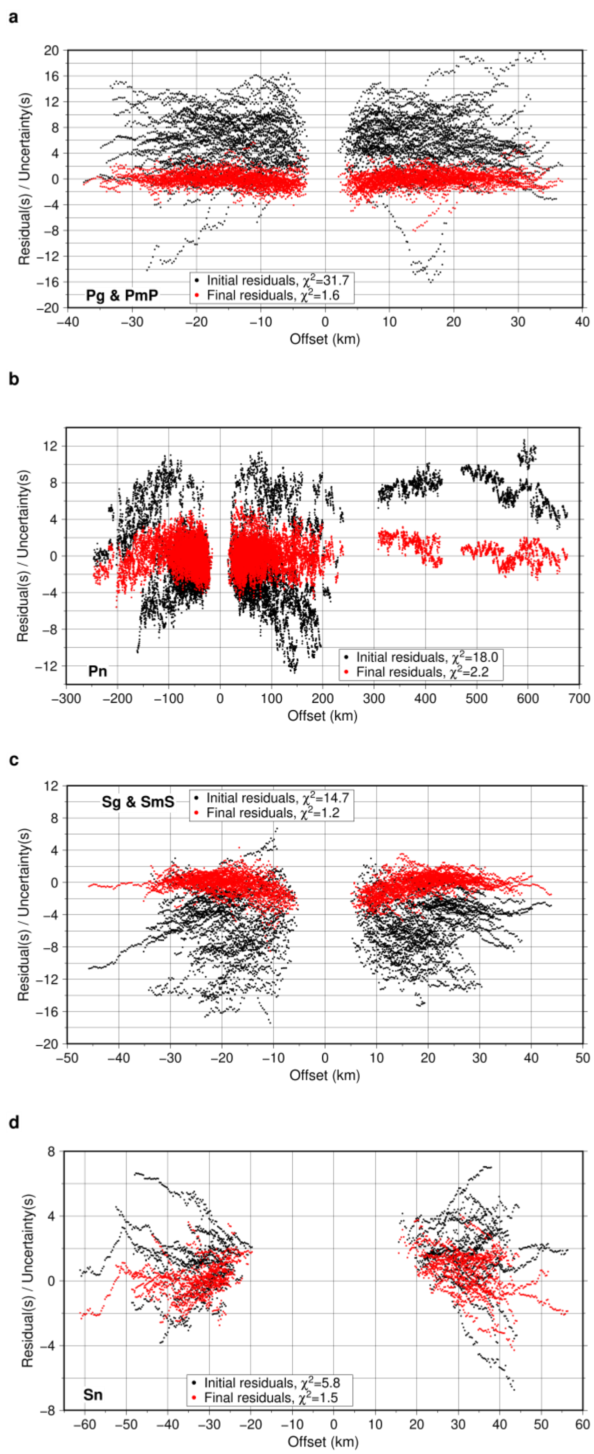


**Supplementary Fig. 3. Normalized travel time residuals as a function of the source-receiver offsets in the initial model (black dots) and the final tomographic model (red dots). a,** Pg and PmP arrivals; **b,** Pn arrivals; **c,** Sg and SmS arrivals; **d,** Sn arrivals.

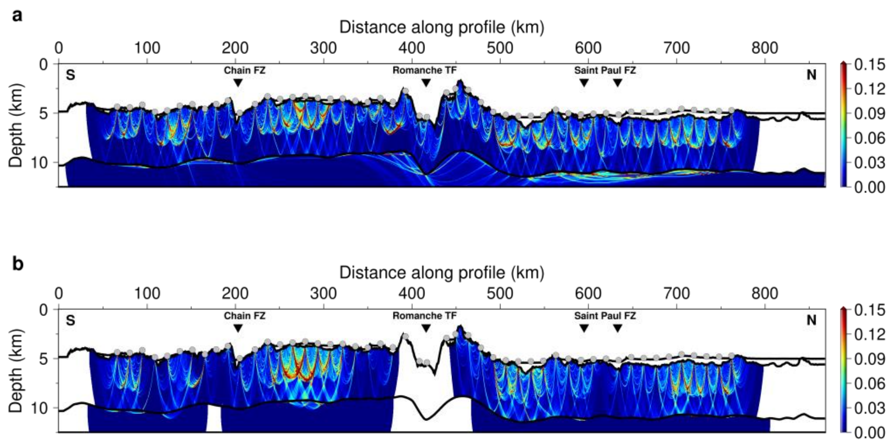


**Supplementary Fig. 4. Density of ray coverage. a**, P-wave arrivals and **b**, S-wave arrivals. The grey circles represent the OBSs.

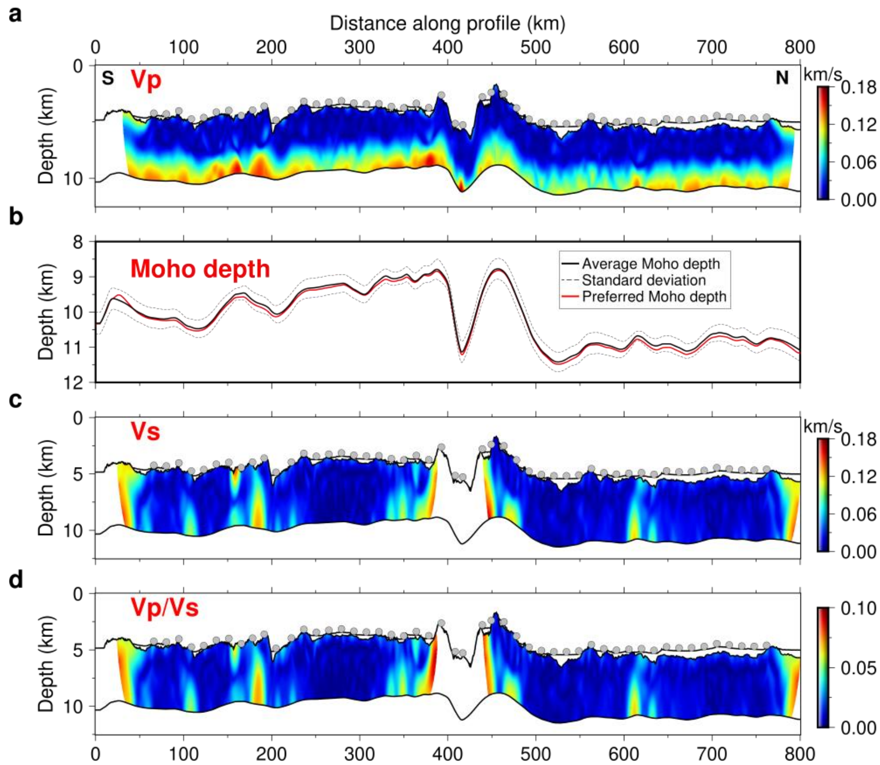


**Supplementary Fig. 5. Model variance using Monte-Carlo analyses. a**, Variance in the crustal Vp. **b**, Variance in the Moho depth. The maximum standard deviation of the Moho depth is ~330 m. **c**, Variance in the crustal Vs. **d**, Variance in the crustal Vp/Vs ratio. The grey circles represent the OBSs.

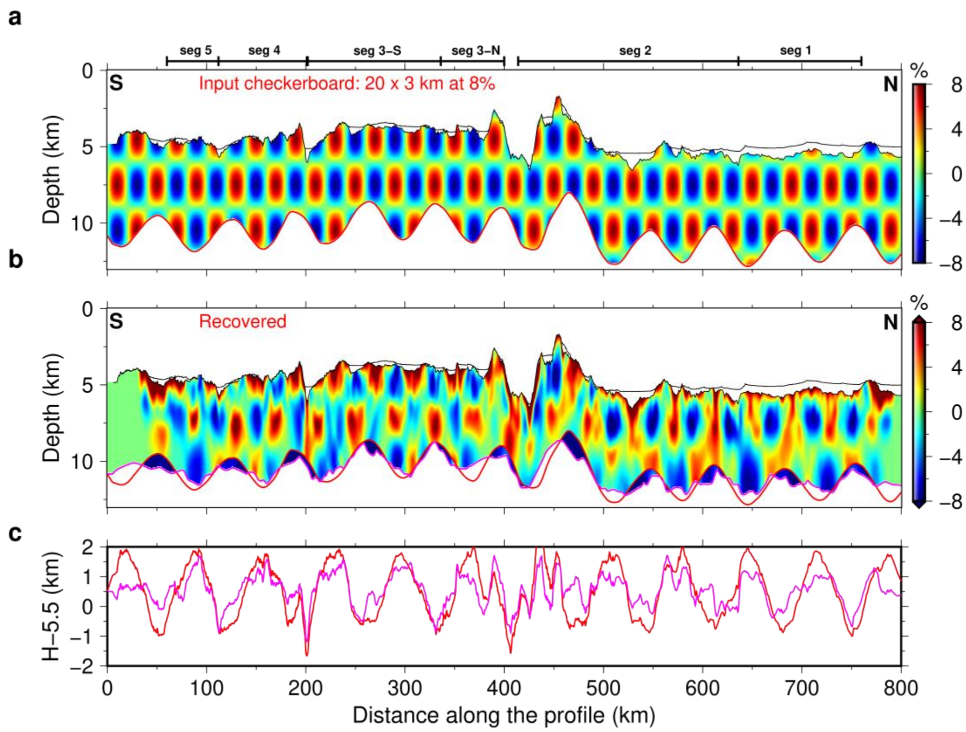


**Supplementary Fig. 6. Checkerboard test for crustal Vp. a**, The input checkerboard pattern with maximum velocity perturbation of ±8% in 20×3 km anomaly size. **b**, The recovered velocity anomalies using the same tomography method as that for the picked Pg and PmP travel times. The red and magenta curves represent the Moho in the checkerboard model and the recovered Moho after tomography, respectively. **c**, Comparison of the real crustal thickness in the checkerboard model (in red) and the recovered crustal thickness after tomography (in magenta).

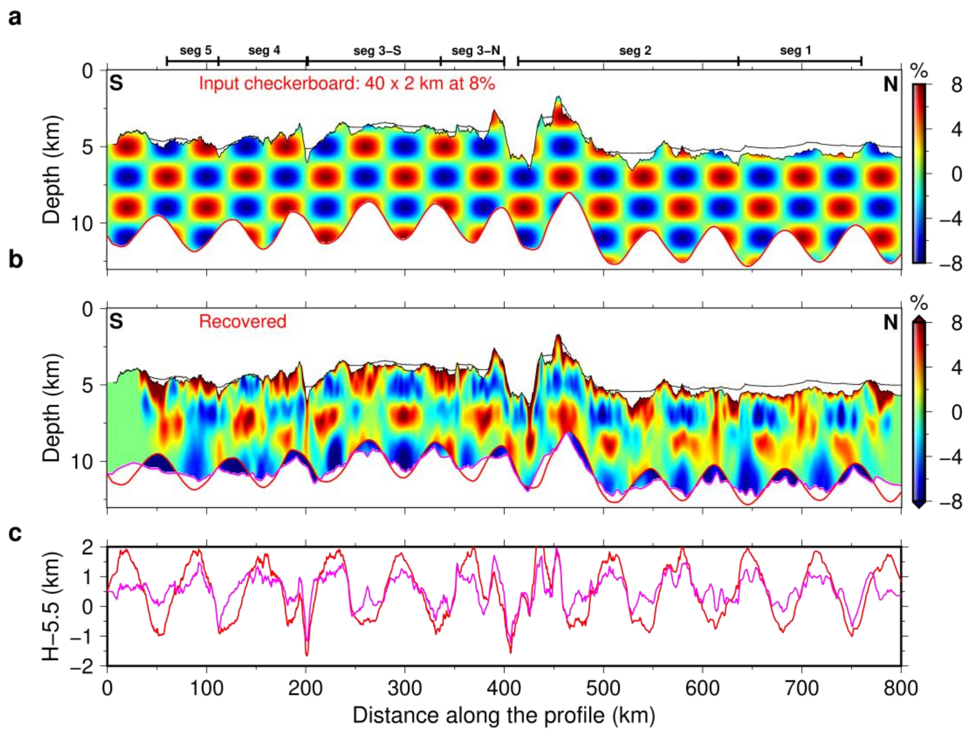


**Supplementary Fig. 7. Checkerboard test for crustal Vp . a**, The input checkerboard pattern with maximum velocity perturbation of ±8% in 40×2 km anomaly size. **b**, The recovered velocity anomalies using the same tomography method as that for the picked Pg and PmP travel times. The red and magenta curves represent the Moho in the checkerboard model and the recovered Moho after tomography, respectively. **c**, Comparison of the real crustal thickness in the checkerboard model (in red) and the recovered crustal thickness after tomography (in magenta).

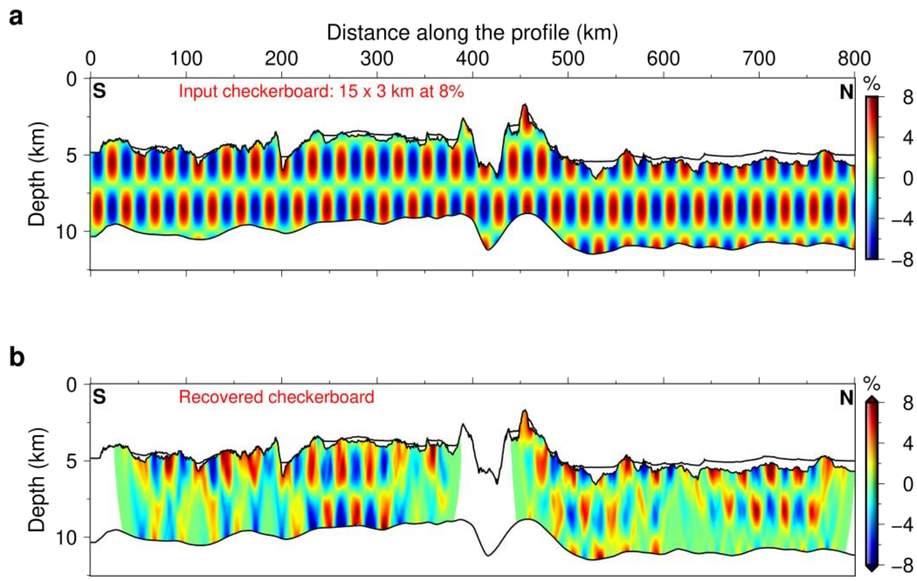


**Supplementary Fig. 8. Checkerboard test for crustal Vs. a**, The input checkerboard pattern with maximum velocity perturbation of ±8%. The size of the velocity anomaly is of 15×3 km. **b**, The recovered velocity anomalies using the same tomography method as that for the picked Sg and SmS travel times.

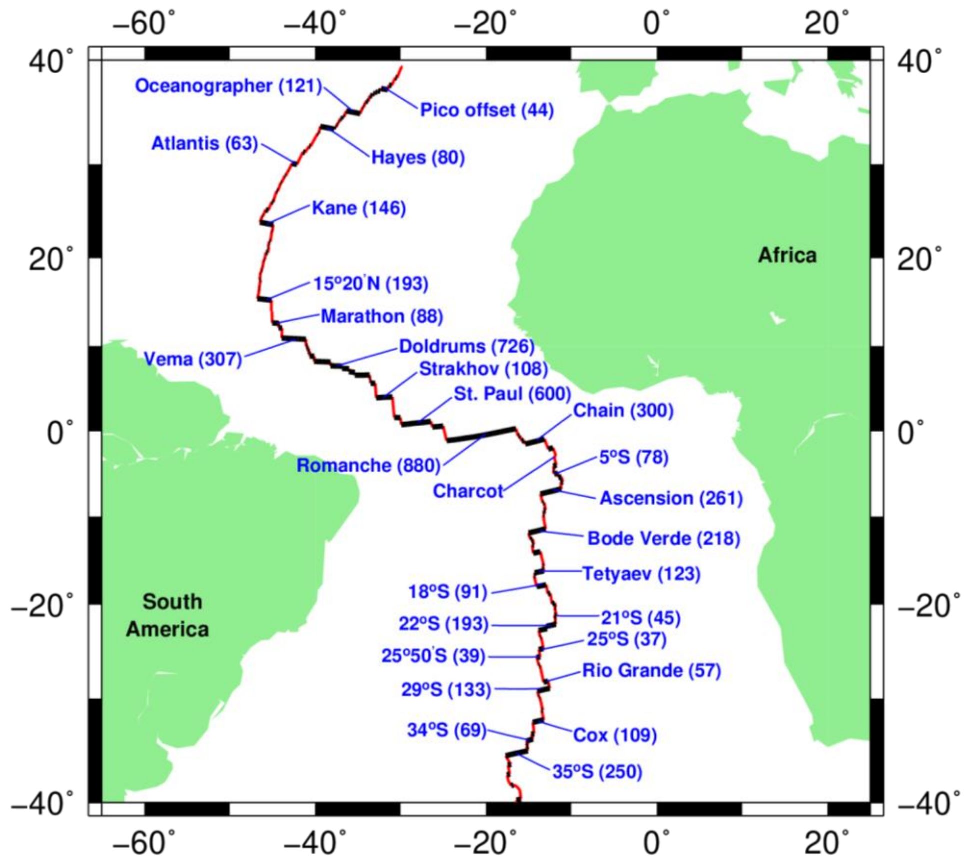


**Supplementary Fig. 9. Map showing the locations and lengths of oceanic transform faults in the Atlantic Ocean between 40°N and 40°S.** The numbers in brackets are the lengths of the transform faults with unit in km. Only transform faults with length >30 km are plotted. For a transform fault composed of several intra-transform faults, the total length of the transform fault is labelled.

**Supplementary Table 1. Interpreted average thicknesses and average vertical Vp gradients of crustal Layer 2 and 3.** The vertical Vp gradient of 0.5 $s^{-1}$ is used as the Layer 2/3 boundary[1]. The errors represent the standard deviations.

| | Thickness of Layer 2 (km) | Average Vp gradient of Layer 2 ($s^{-1}$) | Thickness of Layer 3 (km) | Average Vp gradient of Layer 3 ($s^{-1}$) |
|---|---|---|---|---|
| **Segment 1** | 2.1 ±0.2 | 0.76 ±0.12 | 3.3 ±0.2 | 0.15 ±0.04 |
| **Segment 2** | 2.2 ±0.6 | 0.67 ±0.14 | 3.4 ±0.6 | 0.17 ±0.07 |
| **Segment 3-S** | 1.9 ±0.7 | 0.66 ±0.26 | 3.5 ±0.7 | 0.17 ±0.05 |
| **Segment 4** | 2.3 ±0.6 | 0.80 ±0.19 | 3.1 ±0.6 | 0.15 ±0.10 |
| **Segment 5** | 2.2 ±0.3 | 0.73 ±0.12 | 3.4 ±0.3 | 0.13 ±0.04 |

**Supplementary Table 2. Crustal thickness at the center and ends of segments along the slow-spreading Mid-Atlantic ridge and fast-spreading East Pacific Rise.** The crustal thickness data from the Atlantic Ocean are selected following two criteria: (1) systematically along-axis crustal thinning is observed within the second-order ridge segment and (2) the crustal thicknesses at segment centre and at least one segment end are measured.

| Ocean | Location of ridge (reference) | Name of ridge or seismic profile | Spreading half rate (mm/yr) | Age of crust (Myr) | Crustal thickness at segment center (km) | Crustal thickness at segment end(s) (km) |
|---|---|---|---|---|---|---|
| North Atlantic Ocean | 52 °N[2] | Profile 10617 | 12.7 | ~5.1 | 8 | 5.0 |
| | 33-35°N[3] | OH-1 | ~11 | 0 | 8.2 | 5.0 / 5.0 |
| | | OH-2 | | 0 | 6.9 | 3.3 / 4.4 |
| | | OH-3 | | 0 | 6.6 | 2.5 / 4.2 |
| | 35°N[4] | OH-1 | | ~2 | 8.1 | 3.8 /4.6 |
| | | OH-2 | | ~2 | 7.0 | 3.8 |
| | 35°N[5] | OH-1 | | ~2 | 9.0 | 4.5 / 6.0 |
| | | OH-1 | | ~5 | 6.0 | 3.2 / 3.5 |
| | 21.5°N[6] | TAMMAR | ~13 | 0 | 8.0 | 4.0 / 5.5 |
| | 14.5°N[7] | Segment 4 | ~23 | ~70 | 7.6 | 4.2 / 5.3 |
| South Atlantic Ocean | 33°S[8] | | ~18 | 0 | 7.8 | 3.5 |
| | 8-9°S[9] | segment A2 | ~16 | ~0 | 10 | 6.0 / 7.0 |
| | 5°S[10] | Profile 10 | ~16 | ~0.8 | 8.5 | 2.8 / 3.5 |
| East Pacific Ocean | 15°N[11] | Line 1<br>Line 2 | ~46.5 | 0.8-2.0 | 6.0 | 5.4 |
| | 14.3°N[12] | CLASSIC deployment 1 | ~55 | 0.6-0.9 | 5.8 | 5.6 |
| | 8°15'–10°5'N[13] | Southern segment on Cocos Plate | ~55 | 0.3 | 6.8 | 5.3 |
| | | Northern segment on Cocos Plate | | 0.3 | 7.3 | ~6.0 |
| | 3.5°–5°N[14] | G3 profile | ~70 | 0.58-2 | 6.6 | 5.0 |
| | | Q1 profile | | 0.28-1.42 | 6.0 | 5.0 |

**Supplementary Table 3. Maximum crustal thickness variation between centre and ends of second-order ridge segments and the length of the corresponding first-order ridge segment in the Atlantic Ocean.** The locations of the transform faults are shown in Supplementary Fig. 9.

| **Transform faults bound the first-order ridge segment** | **Length of the first-order segment (km)** | **Maximum crustal thickness variation within the segment (km)** | **Age of the measured crust (Myr)** |
|---|---|---|---|
| Pico Offset—Oceanographer TF | ~360 | 4.0[15] | 0 |
| Oceanographer TF—Hayes TF | ~220 | 4.1[3] | 0 |
| | | 4.3[4] | ~2 |
| | | 2.8[5] | ~5 |
| Atlantis TF—Kane TF | ~800 | 3.5[16] | 0 |
| Kane TF—15°20'N TF | ~930 | 4.0[6] | 0 |
| 15°20'N TF—Marathon TF | ~270 | 3.4[7] | ~65 |
| Charcot TF—5°S TF | ~230 | 5.7[10] | ~0.8 |
| Ascension TF—Bode Verde TF | ~450 | 4.0[9] | 0 |
| Cox TF— 34°S TF | ~190 | 4.3[8] | 0 |

**Supplementary Table 4. Lengths of oceanic TFs and NTOs in the Atlantic Ocean and the crustal thinning towards these TFs and NTOs.** Only the crustal thickness constrained by active-source seismic data is considered.

| TF or NTO | Length of TF or NTO (km) | Location of the measured crust | Age of crust (Myr) | Crustal thickness at segment center (km) | Crustal thickness at TF or NTO (km) |
|---|---|---|---|---|---|
| Charlie-Gibbs TF | ~350 | South of TF | ~5.1 | 8 | 5.0[2] |
| Oceanographer TF | ~121 | South of TF | 0 | 8.2 | 5.0[3] |
| | | | ~2 | 8.1 | 4.6[4] |
| | | | ~2 | 9.0 | 4.5[5] |
| | | | ~5 | 6.0 | 3.5[5] |
| NTO-1 at 34.5°N | ~35 | South of NTO-1 | 0 | 6.9 | 3.3[3] |
| | | | ~2 | 7.0 | 3.8[4] |
| | | North of NTO-1 | 0 | 8.2 | 5.0[3] |
| | | | ~2 | 8.1 | 3.8[4] |
| | | | ~2 | 9.0 | 6.0[5] |
| | | | ~5 | 6.0 | 3.2[5] |
| NTO-2 at 34°N | ~35 | South of NTO-2 | 0 | 6.6 | 4.2[3] |
| | | North of NTO-2 | 0 | 6.9 | 4.4[3] |
| NTO-3 at 33.5°N | ~15 | North of NTO-3 | 0 | 6.6 | 2.5[3] |
| Marathon TF | ~88 | North of TF | ~70 | 7.6 | 5.3[7] |
| Ascension TF | ~261 | South of TF | 0 | 10 | 6.0[9] |
| 5°S TF | ~70 | North of TF | ~0.8 | 8.5 | 2.8[10] |

# Reference


1. Vaddineni, V. A., Singh, S. C., Grevemeyer, I., Audhkhasi, P. & Papenberg, C. Evolution of the Crustal and Upper Mantle Seismic Structure From 0 – 27 Ma in the Equatorial Atlantic Ocean at 2° 43′ S. *J. Geophys. Res.* **126**, e2020JB021390 (2021).

2. Whitmarsh, R. B. & Calvert, A. J. Crustal structure of Atlantic fracture zones — I. The Charlie-Gibbs Fracture Zone. *Geophys. J. Int.* **85**, 107-138 (1986).

3. Hooft, E. E. E., Detrick, R. S., Toomey, D. R., Collins, J. A. & Lin, J. Crustal thickness and structure along three contrasting spreading segments of the Mid-Atlantic Ridge, 33.5°–35°N. *J. Geophys. Res.* **105**, 8205-8226 (2000).

4. Canales, J. P., Detrick, R. S., Lin, J., Collins, J. A. & Toomey, D. R. Crustal and upper mantle seismic structure beneath the rift mountains and across a nontransform offset at the Mid-Atlantic Ridge (35°N). *J. Geophys. Res.* **105**, 2699-2719 (2000).

5. Sinha, M. C. & Louden, K. E. The Oceanographer fracture zone — I. Crustal structure from seismic refraction studies. *Geophys. J. Int.* **75**, 713-736 (1983).

6. Dannowski, A., et al. Crustal structure of the propagating TAMMAR ridge segment on the Mid-Atlantic Ridge, 21.5°N. *Geochem. Geophys. Geosyst.* **12**, Q07012 (2011).

7. Davy, R. G., Collier, J. S., Henstock, T. J. & Consortium, T. V. Wide-Angle Seismic Imaging of Two Modes of Crustal Accretion in Mature Atlantic Ocean Crust. *J. Geophys. Res.* **125**, e2019JB019100 (2020).

8. Tolstoy, M., Harding, A. J. & Orcutt, J. A. Crustal Thickness on the Mid-Atlantic Ridge: Bull's-Eye Gravity Anomalies and Focused Accretion. *Science* **262**, 726-729 (1993).

9. Minshull, T. A., Bruguier, N. J. & Brozena, J. M. Ridge-plume interactions or mantle heterogeneity near Ascension Island? *Geology* **26**, 115-118 (1998).

10. Planert, L., Flueh, E. R. & Reston, T. J. Along- and across-axis variations in crustal thickness and structure at the Mid-Atlantic Ridge at 5°S obtained from wide-angle seismic tomography: Implications for ridge segmentation. *J. Geophys. Res.* **114**, B09102 (2009).

11. Tréhu, A. M. & Purdy, G. M. Crustal structure in the Orozco Transform Zone. *J. Geophys. Res.* **89**, 1834-1842 (1984).

12. Van Avendonk, H. J. A., Harding, A. J., Orcutt, J. A. & McClain, J. S. A two-dimensional tomographic study of the Clipperton transform fault. *J. Geophys. Res.* **103**, 17885-17899 (1998).

13. Pablo Canales, J., Detrick, R. S., Toomey, D. R. & Wilcock, W. S. D. Segment-scale variations in the crustal structure of 150 – 300 kyr old fast spreading oceanic crust (East Pacific Rise, 8° 15′ N – 10° 5′ N) from wide-angle seismic refraction profiles. *Geophys. J. Int.* **152**, 766-794 (2003).

14. Roland, E., Lizarralde, D., McGuire, J. J. & Collins, J. A. Seismic velocity constraints on the material properties that control earthquake behavior at the Quebrada-Discovery-Gofar transform faults, East Pacific Rise. *J. Geophys. Res.* **117**, B11102 (2012).

15. Detrick, R. S., Needham, H. D. & Renard, V. Gravity anomalies and crustal thickness variations along the Mid-Atlantic Ridge between 33 °N and 40 °N. *J. Geophys. Res.* **100**, 3767-3787 (1995).

16. Lin, J., Purdy, G. M., Schouten, H., Sempere, J. C. & Zervas, C. Evidence from gravity data for focused magmatic accretion along the Mid-Atlantic Ridge. *Nature* **344**, 627-632 (1990).